Intelligent Radiomic Analysis of Q-SPECT/CT images to optimize pulmonary embolism diagnosis in COVID-19 patients

Debora Gil
Computer Vision Center (CVC),
Computer Sci. Dept., UAB.
Barcelona, Spain.
{debora,csanchez,gtorres}@cvc.uab.cat

Sonia Baeza
Resp. Med. Dep., HUGTiP,
IGTP Res. Inst.
Med. Dept., UAB.
Barcelona, Spain
smbaeza.germanstrias@gencat.cat

Carles Sanchez
Computer Vision Center (CVC),
Computer Sci. Dept., UAB.
Barcelona, Spain.
csanchez@cvc.uab.cat

Guillermo Torres
Computer Vision Center (CVC),
Computer Science Dept., UAB.
Barcelona, Spain.
gtorres@cvc.uab.cat

Ignasi García-Olivé
Resp. Med. Dept., HUGTiP,
IGTP Res. Inst.,
CIBERES,
Med. Dept., UAB.
Barcelona, Spain
igarcia.germanstrias@gencat.cat

Gloria Moragas
Nuc. Med. Dept., HUGTiP,
Barcelona, Spain.
gmoragas.germanstrias@gencat.cat

Jordi Deportós
Nuc. Med. Dept., HUGTiP,
Barcelona, Spain.
jordi.deportos.idi@gencat.cat

Maite Salcedo
Nuc. Med. Dept., HUGTiP,
Barcelona, Spain.
maitesalcedo@hotmail.com

Antoni Rosell
Resp. Med. Dept., HUGTiP,
IGTP Res. Inst.,
CIBERES,
Med. Dept., UAB.
Barcelona, Spain
arosellg.germanstrias@gencat.cat

Abstract

Coronavirus disease 2019 (COVID-19) pneumonia is associated with a high rate of pulmonary embolism (PE). In patients with contraindications for CT pulmonary angiography (CTPA) or non-diagnostic on CTPA, perfusion single photon emission computed tomography/computed tomography (Q-SPECT/CT) is a diagnosis option. The goal of this work is to develop an Intelligent Radiomic system for the detection of PE in COVID-19 patients from the analysis of Q-SPECT/CT scans.

Our Intelligent Radiomic System for identification of patients with PE (with/without pneumonia) is based on a local analysis of SPECT-CT volumes that considers both CT and

SPECT values for each volume point. We present an hybrid approach that uses radiomic features extracted from each scan as input to a siamese classification network trained to discriminate among 4 different types of tissue: no pneumonia without PE (control group), no pneumonia with PE, pneumonia without PE and pneumonia with PE.

The proposed radiomic system has been tested on 133 patients, 63 with COVID-19 (26 with PE, 22 without PE, 15 indeterminate-PE) and 70 without COVID-19 (31 healthy/control, 39 with PE). The per-patient recall for the detection of COVID-19 pneumonia and COVID-19 pneumonia with PE was, respectively, 91% and 81% with an area under the receiver operating characteristic curves equal to 0.99 and 0.87.

1. Introduction

Coronavirus disease 2019 (COVID-19) pneumonia is associated with hyperinflammatory syndrome [8, 18] as well as coagulation abnormalities and thrombosis [13, 10, 1], highlighting a higher incidence of pulmonary embolism (PE) [12, 21, 24, 11, 7] whose diagnosis can be challenging.

CT pulmonary angiography (CTPA) is the most widely used imaging test for PE diagnosis [20, 27] but in patients with contraindications (allergy to iodinated contrast, kidney failure) or nondiagnostic on CTPA, another test is necessary. The role of ventilation/perfusion SPECT/CT has decreased because in patients with COVID-19 the use of ventilation is discouraged due to the high risk of aerosol production [27, 28]. Due to the need to adapt this test based on security standards required by the pandemic, perfusion single photon emission computed tomography/computed tomography (Q-SPECT/CT) is a diagnosis option in patients with COVID-19 disease [3, 2, 16].

Q-SPECT/CT can be difficult to interpret, especially in the presence of associated pulmonary infiltrates. Also a main challenge in COVID-19 pathology diagnosis is the accurate localization of the injured tissue inside the lung. As a consequence, radiological diagnosis often need to be validated by two senior nuclear physicians. An artificial intelligence system to support radiologists in the diagnosis of PE through Q-SPECT/CT would improve the sensitivity of PE diagnosis in cases of associated pneumonia, and reduce the reading time of the test.

Early detection of COVID-19 from medical imaging has risen great interest within the artificial intelligence community. However, to the best of our knowledge, currently there are no published studies that use artificial intelligence to improve the diagnosis of COVID-19 PE through Q-SPECT/CT.

Existing methods addressing diagnosis of COVID-19 pathologies mainly focus on the detection of COVID-19 pneumonia from the analysis of a single modality (either X-ray or CT scans). The majority of methods are deep learning approaches based on well-known architectures successful in other fields (like ResNet [14], U-net [17] or EfficientNet [9], among others) that are adapted and fine tuned for managing COVID-19 diagnosis.

Regardless of the imaging modality and architecture, the usual approach is to use a classification scheme that provides a single diagnosis for each image/scan [19, 5]. Patients with severe COVID-19 have several lung pathologies at the same time and a main challenge is its accurate localization inside lungs. It follows that a classification scheme yielding a single diagnosis from the analysis of the whole image/scan might have some limitations for a successful clinical use.

A single diagnosis based on analysis of whole images/scans might only detect the main pathology and ignore the secondary ones which are also clinically relevant. Another issue is the clinical interpretability of results. Although it can be improved with the use of a heatmap (like the gradient-weighted class activation mapping [23]), deep learning approaches are still difficult to interpret and lack of the ability to accurately locate the injured tissue.

Another concern recently identified [4] is the sensitivity of models to the quality and quantity of the cases used for training and testing, which can lead to overestimating results. Deep learning methods require a large number of annotated images for training. While this is not a major issue in most fields of application, in the case of COVID-19, there is a limited availability of images and it is suspected that its origin and protocol of acquisition can introduce bias in models [26]. In particular, it is reported [6] that the high-performance could be mainly attributed to the presence of image patterns (like corner labels or instrumentation), device acquisition parameters or population factors (like sex or age). In case such characteristics are specific for some of the classes (groups of patients), models could learn to recognizing these biases in the data set, rather than focusing on the pathologies they are trying to detect. This bias, of course, limits the generalization and reproducibility of results when tested on data sets with a different origin from the ones used in training and tested.

We consider that adopting a local approach analyzing tissue regions instead of the whole scan could alleviate the need for a large number of annotated cases, as well as, minimize the impact of biases in the images. This work presents an artificial intelligence (AI) model based on Q-SPECT/CT images of patients for the identification of local lung lesions associated to COVID-19 pathologies. Our system bases on a local analysis of SPECT-CT volumes to identify four clinically relevant types of tissue defined by nuclear medicine: healthy, pulmonary embolism, pneumonia and pneumonia with pulmonary embolism.

We present an hybrid approach that uses radiomic features extracted from each scan as input to a siamese classification network trained from scratch. The radiomic features are a selection of PyRadiomics 1st order and texture descriptors that are reproducible under variations in the acquisition protocol and medical scan parameters. Experiments on 133 cases (including 63 prospective COVID-19 patients) of an own data set show a per-patient recall for the detection of COVID-19 pneumonia and COVID-19 pneumonia with PE was, respectively, 91% and 81% with an area under the receiver operating characteristic curves equal to 0.99 and 0.87.

2. COVID-19 DataSet

This is a single center study with a prospective observational branch with patients who tested positive for COVID-19 and a retrospective branch with patients in prepandemic period. Patients from both branches underwent a Q-SPECT/CT study for diagnosis of PE. The prospective observational branch was collected from April 2020 to September 2020, while the retrospective branch was from patients without COVID-19 infection who underwent perfusion SPECT-CT studies for the diagnosis of PE between January 2018 and December 2018. The only exclusion criterions were the patient's refusal to participate in the study and the detection of severe alterations in the patients' lungs caused by other pathologies non related to COVID-19 infection.

The total number of patients from which imaging data was acquired was 148. From these, a total of 15 cases were discarded due to technical failures of the image acquisition process or to the presence of severe alterations in the patients' lungs caused by other pathologies non related to COVID-19 infection. This way, the resulting database contained data a total of 133 patients were collected, 63 in prospective branch (26 with PE, 22 without PE, 15 indeterminate-PE) and 70 in retrospective branch (31 healthy/control, 39 PE).

Patients data was collected and classified in the following five groups: 1) Patients without COVID-19 nor PE (control). 2) Patients without COVID-19 and with PE (PE-noCOVID). 3) Patients with COVID-19 and without PE (noPE-COVID). 4) Patients with COVID-19 and with PE (PE-COVID). 5) Patients with COVID-19, suspected of having PE but without imaging-confirmed diagnosis (suspectedPE-COVID).

The classification of the different cases and different tissue type segments was performed by a team of pneumologists and nuclear medicine physicians of Germans Trias i Pujol University Hospital. A total number of 8233 tissue samples from 20 subjects were manually annotated using an own-developed software.

For each patient, a perfusion single photon emission computed tomography/computed tomography (Q-SPECT/CT) based on intravenous administration of 6 mCi (222 MBq) of 99mCt-macroaggregates of human albumin (99mCt-MAA) was acquired, with the subsequent acquisition of a tomo-scintigraphy (SPECT) and a CT in two hybrid equipments indistinctly: a Symbia T2 Gamma camera (brand Siemens, based in Munich, Germany) and a Discovery NM/CT 670 ES Gamma camera (brand General Electric, based in Boston, Massachusetts, US). The acquisition parameters were the following.

The SPECT was obtained with a circular orbit with 360°arc, 128x128 matrix, zoom 1, 140 KeV photopeak, obtaining 90 images of 8 seconds per image. The acquired CTs used 120 KV, 50-350 mA, with slice thickness and interval of 1.25 mm (General Electric) and 3 mm (Siemens). With reconstructions of B41S, B80S, B08 and 1 soft, recon 2 lung respectively for CT and three-dimensional reconstruction, without attenuation correction for scintigraphy, 512x512 matrix. Ventilation lung scintigraphy was not contemplated due to the risk of cross-contamination of COVID, so ventilation alterations were determined by CT scans.

3. Intelligent Radiomics for Detection of PE in COVID-19 Patients

The proposed radiomic system analyzes the intensity values of CT and SPECT volumes for each voxel in order to discriminate four clinically relevant types of tissue defined by nuclear medicine experts:

1. Control: healthy tissue (normal CT and SPECT).
2. NoNeumo PE: classic PE (normal CT with a localized perfusion defect in the SPECT).
3. Neumo NoPE: pneumonia with normal perfusion (affected CT but normal per-fusion in the area).
4. Neumo PE: pneumonia with affected perfusion (area with affectations in both the CT and SPECT scans).

In order to avoid over fitting, two extra categories were added:

5. Black Background: areas with no tissue uptake.
6. Body Tissue: areas of the body not belonging to the lungs.

Our intelligent radiomic system has three main steps. Since the final diagnostic requires the combination of information from the SPECT and CT scans, the first step consists in the registration of the two volumes in order to fuse both image modalities. Second, radiomic features selected according to its reproducibility are extracted from the registered volumes to define a radiomic feature space. Finally, a

machine learning method is used to disseminate each value of the feature space between the four types of tissue.

In order to register volumes, first SPECT volumes were resized to match the same number of CT slices using HOROS, an open source medical image viewer REF. Then, we used an affine monomodal transformation REF to register a seg-mentation of the lungs in CT and SPECT resized volumes. By registering binary masks instead of intensity volumes, we can account for multimodal differences using the Mean Squared Error as cost function and, thus, minimize the risk of premature convergence that multimodal approaches using mutual information have. The computed transformation was applied to intensity SPECT volumes to register them to CT scans.

The segmentation of lungs was computed using thresholding and morphological operations. CT lungs were selected as the larger connected component of the voxels with intensity between 950 to -300 Hounsfield Units, followed by a closing with a structuring element of size 5. For the lung segmentation of the perfusion volumes, a threshold of intensity 20 was selected.

The radiomic features are a subset of PyRadiomics [25], an open-source python package for the extraction of Radiomics features from medical imaging volumes. PyRadiomics features include shape features, first order features, and textural features (Gray Level Co-ocurrence Matrix (GLCM), Gray Level Size Zone (GLSZM), Gray Level Run Length Matrix (GLRLM) and Gray Level Dependency Matrix (GLDM)) describing several aspects of the lesion. The subset was selected according to the reproducibility against different image acquisition conditions and inter-observer variability in lesion identification. Reproducibility bases on the correlation of feature values obtained from data collected using different conditions and settings [15]. The selected set of (17) features are given in Table 1.

For each pixel and scan, the reproducible radiomic features were computed in windows of size $sze \times sze$. These features are the input to a fully connected simaese network that combines them in a multi-classification approach. Each siamese network has two fully connected layers with 128 neurons linked with one relu layer and an output classification layer with sigmoid activation. The output of the classification layers for the two networks is concatenated to define a 12 (2×6 classes) dimensional vector that it is the input to a fully connected layer with sigmoid activation. To account for unbalancing in training data, the loss function is a weighted cross entropy given by:

$$\text{loss} = \frac{\sum_{i=1}^{N} weight[class[i]] loss(i, class[i])}{\sum_{i=1}^{N} weight[class[i]]} \quad (1)$$

where $loss(i, class[i])$ is the cross-entropy loss for the i-th class computed from the classifier prediction x and the true class as:

$$\text{loss}(x, class) = -\log\left(\frac{\exp(x[class])}{\sum_{j=1}^{N}\exp(x[j])}\right) \quad (2)$$

and the weight $weight[class[i]]$ is given by the inverse of the class frequency.

4. Experiments

In order to statistically validate the system, we used a leave-one-out patient validation. To assess performance, for each of the 4 types of pulmonary tissues, receiver operating characteristic (ROC) curves were plotted and the area under the curve (AUC), precision and recall were computed. If TP_i, FP_i, FN_i, denote, respectively, the true and false positives and the false negatives for the i-th tissue type, then its precision, $PREC_i$, and recall, REC_i are given by:

$$REC_i = 100\frac{TP_i}{TP_i + FN_i} \quad (3)$$

$$PREC_i = 100\frac{TP_i}{TP_i + FP_i} \quad (4)$$

In order to assess the impact of the size of the window used to compute radiomic features, we trained two different models with features extracted using windows of size: $sze \times sze = 3 \times 3$ and $sze \times sze = 5 \times 5$.

Tables 2 and 3 report the ranges (given by the average +/- the standard deviation) for Recall and Precision of each tissue type and models using 3×3 and 5×5 windows, respectively. The average recall and precision for COVID-19 pneumonia tissue are 91% and 100% for 3×3 windows and 96% and 100% for 5×5 windows. The average recall and precision for tissue affected of COVID-19 pneumonia with PE are 81% and 77% for 3×3 windows and 74% and 77% for 5×5 windows.

Figures 1 and 2 show receiver operating characteristic curves with their areas (AUC) for each lung tissue for models using 3×3 and 5×5 windows, respectively. The areas for COVID-19 pneumonia are 0.99 for both models, while the areas for COVID-19 pneumonia with PE are 0.86 for 3×3 windows and 0.89 for 5×5 windows.

5. Discussion and Conclusions

This study represents a first step towards a complete intelligent radiomic system to optimize the diagnosis of PE by Q-SPECT/CT. Diagnosis of complications associated to COVID-19 is challenging for two main issues. First, patients usually present several pathologies at different lung regions simultaneously, which complicates their radiological visual identification. Second, there is a limited availability of annotated data, which hinders the performance of machine and deep learning methods. In order to minimize

Table 1. Features selected according to reproducibility

Firstorder	Texture GLCM	Texture GLDM	Texture GLRLM
Entropy TotalEnergy Uniformity	Id Idm JoinEnergy MaximumProbability	Dependence Non Uniformity Normalized Dependence Variance Large Dependence Emphasis	Gray Level Non Uniformity Normalized Run Length Non Uniformity Normalized Run Percentage Short Run Emphasis

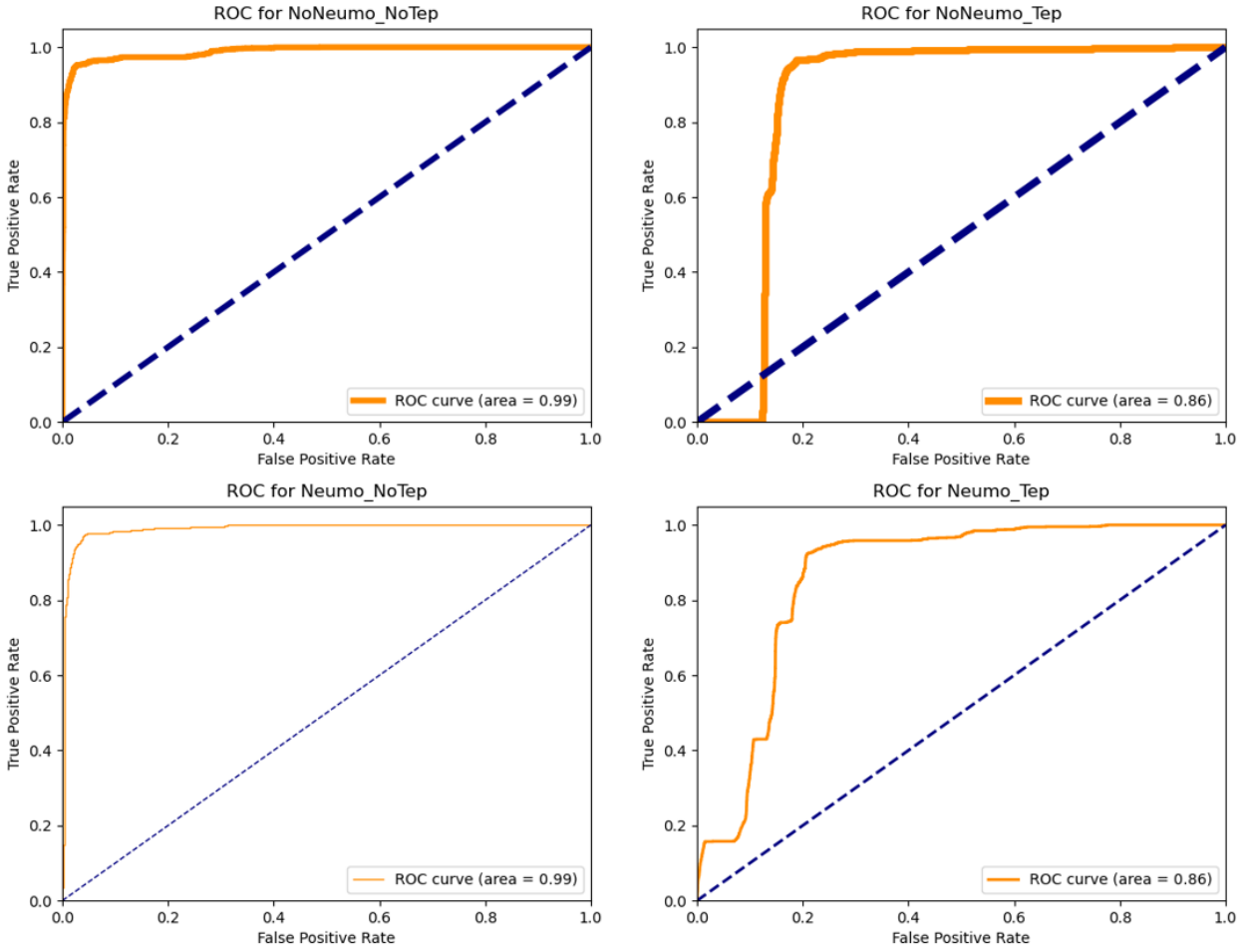

Figure 1. ROC curves of the model with features computed in 3x3 windows.

Table 2. Ranges (mean +/- SD) for Recall and Precision of each tissue type. Model computed using 3x3 windows

	No Pneumonia		Pneumonia	
	No PE	PE	No PE	PE
Recall	92 ± 14	95 ± 4	91 ± 7	81 ± 2
Precision	100 ± 0	82 ± 24	100 ± 0	77 ± 23

Table 3. Ranges (mean +/- SD) for Recall and Precision of each tissue type. Model computed using 5x5 windows

	No Pneumonia		Pneumonia	
	No PE	PE	No PE	PE
Recall	92 ± 14	75 ± 34	96 ± 7	74 ± 5
Precision	100 ± 0	96 ± 5	100 ± 0	77 ± 23

the impact of both issues, we have proposed an hybrid approach that uses traditional radiomic local features as input to a siamese fully connected network that combines extracted data from CT and Q-SPECT scans.

Our method achieves average detections of 91% (0.99 AUC) for tissue with COVID-19 pneumonia and 82% (0.86 AUC) for tissue with COVID-19 pneumonia and PE. The sensitivity for the detection of COVID-19 pneumonia

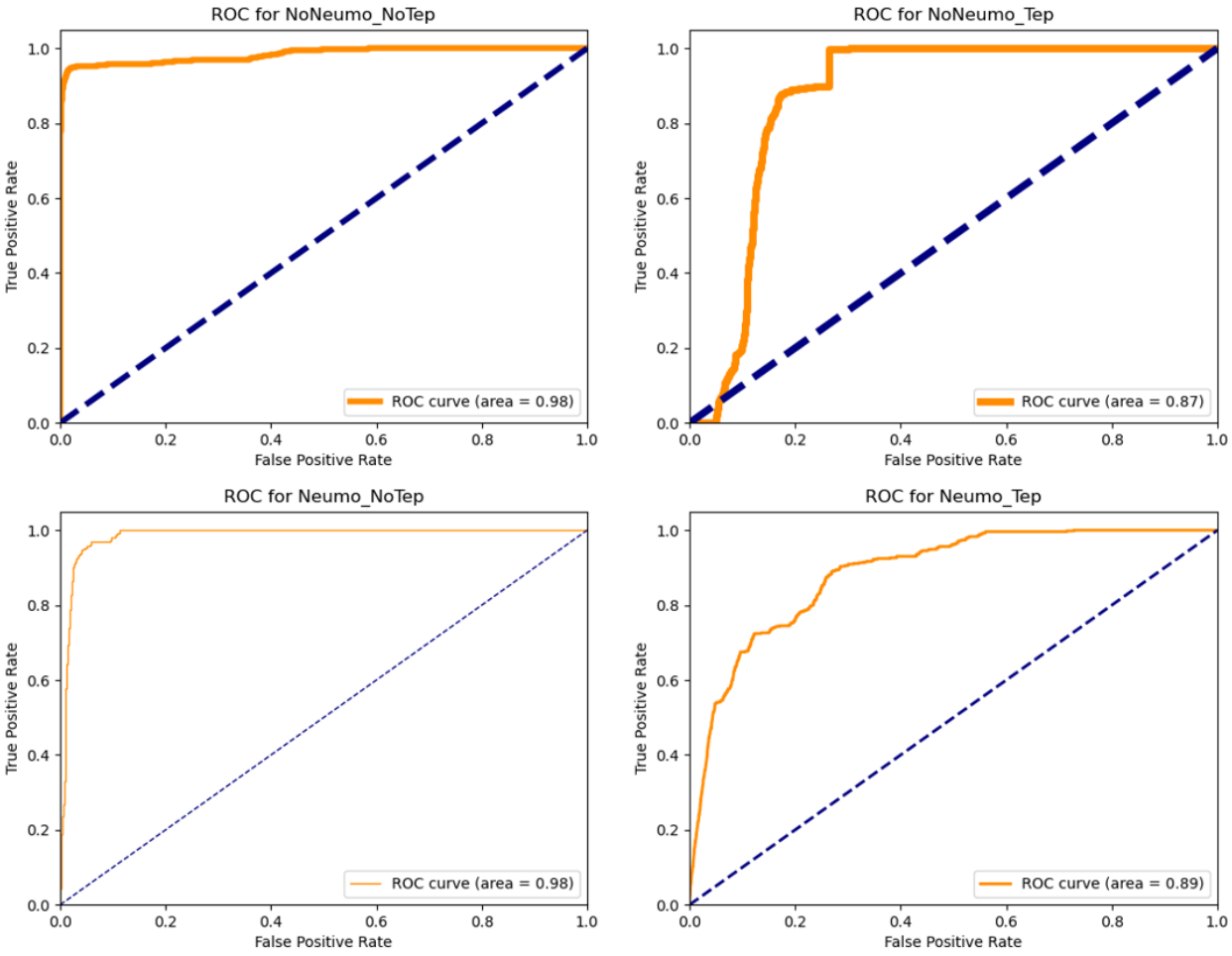

Figure 2. ROC curves of the model with features computed in 5x5 windows.

is comparable to deep learning approaches using a higher number of training cases, like COVNet [14] (90% recall and 0.96 AUC) or the early work of [22] (88% recall and 0.92 AUC). The drop in the detection of COVID-19 pneumonia with PE is mainly due to the fact that tissue affected by COVID-19 PE has a non-uniform pneumonia mixed with other alterations and still functional tissue. It follows that regions labelled as COVID-19 pneumonia with PE are prone to have some parts without pneumonia.

Figure 3 shows an example of a patient affected by COVID-19 pneumonia with PE. The top image shows the CT scan and the bottom one the SPECT perfusion scan. White lung areas in CT scan show low functional tissue with either pneumonia or infiltrations. The triangular dark area in SPECT perfusion scan is a lung segment poorly irrigated due to a PE. The white square highlights the region that has been diagnosed as COVID-19 pneumonia with PE. The middle image close-up clearly shows that tissue with COVID-19 pneumonia with PE has an heterogeneous affectation and still has dark functional areas.

This study has some limitations. First, the local identification of tissue types should be aggregated for each case (similarly to [14]) to produce a multiple clinical diagnosis of all the pathologies that the patient has. Second, models should be tested in the whole set of patients and in cases coming from other hospitals in order to fully validate the generalization capability and clinical applicability of models. Finally, performance in detection of COVID-19 pneumonia and PE could improve with an architecture combining the outcomes of models trained using windows of different sizes.

In conclusion, a hybrid approach can detect COVID-19 pneumonia and COVID-19 pneumonia with PE using a limited number of annotated data. The capability to detect alterations in perfusion for COVID-19 pneumonia encourages developing a tool in the cloud for clinical use.

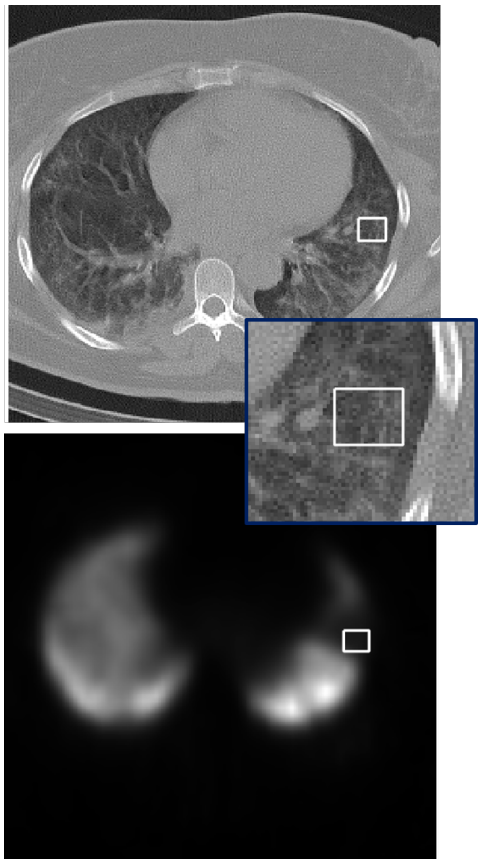

Figure 3. Example of COVID-19 pneumonia with PE. The top image shows the CT scan and the bottom one the SPECT perfusion scan with the region with COVID-19 pneumonia and PE inside the white square. A close-up in the CT scan of such region is shown in the middle image.

6. Acknowledgements

This project is supported by the Spanish Ministry of Science, Innovation and Universities under grant RTI2018-095209-B-C22, RTI2018- 095209-B-C21, Generalitat de Catalunya, 2017-SGR-1624 and CERCA-Programme. Debora Gil is supported by Serra Hunter Fellow.

References

[1] Maximilian Ackermann, Stijn E Verleden, Mark Kuehnel, Axel Haverich, Tobias Welte, Florian Laenger, Arno Vanstapel, Christopher Werlein, Helge Stark, Alexandar Tzankov, et al. Pulmonary vascular endothelialitis, thrombosis, and angiogenesis in covid-19. *New England Journal of Medicine*, 383(2):120–128, 2020. 2

[2] Irene A Burger, Tilo Niemann, Dimitri Patriki, François Fontana, and Jürg-Hans Beer. Is there a role for lung perfusion [99m tc]-maa spect/ct to rule out pulmonary embolism in covid-19 patients with contraindications for iodine contrast?, 2020. 2

[3] Jeeban P Das, Randy Yeh, and Heiko Schöder. Clinical utility of perfusion (q)-single-photon emission computed tomography (spect)/ct for diagnosing pulmonary embolus (pe) in covid-19 patients with a moderate to high pre-test probability of pe. *European journal of nuclear medicine and molecular imaging*, pages 1–6, 2020. 2

[4] J DLopez.Cabrera, R Orozco Morales, J Armando Portal Diaz, and et al. Current limitations to identify covid.19 using artificial intelligence with chest x.ray imaging. *Health and Technology*, 11:411–424, 2021. 2

[5] Shah FM and et al. A comprehensive survey of covid-19 detection using medical images. *https ://engrxiv.org/9fdyp/download/?forma t=pdf.*, 2020. 2

[6] Maguolo G and Nanni L. A critic evaluation of methods for covid-19 automatic detection from x-ray images. *http://arxiv.org/abs/2004.12823*, 2020. 2

[7] Franck Grillet, Julien Behr, Paul Calame, Sébastien Aubry, and Eric Delabrousse. Acute pulmonary embolism associated with covid-19 pneumonia detected with pulmonary ct angiography. *Radiology*, 296(3):E186–E188, 2020. 2

[8] Joshua N Gustine and Dennis Jones. Immunopathology of hyperinflammation in covid-19. *The American Journal of Pathology*, 2020. 2

[9] Bai HX, Wang R, Xiong Z, and et al. Artificial intelligence augmentation of radiologist performance in distinguishing covid-19 from pneumonia of other origin at chest ct. *Radiology*, 296(3):E156–E165, 2020. 2

[10] Toshiaki Iba, Jerrold H Levy, Marcel Levi, and Jecko Thachil. Coagulopathy in covid-19. *Journal of Thrombosis and Haemostasis*, 18(9):2103–2109, 2020. 2

[11] Davide Ippolito, Teresa Giandola, Cesare Maino, Anna Pecorelli, Carlo Capodaglio, Maria Ragusi, Marco Porta, Davide Gandola, Alessandro Masetto, Silvia Drago, et al. Acute pulmonary embolism in hospitalized patients with sars-cov-2-related pneumonia: multicentric experience from italian endemic area. *La radiologia medica*, pages 1–10, 2021. 2

[12] FA Klok, MJHA Kruip, NJM Van der Meer, MS Arbous, DAMPJ Gommers, KM Kant, FHJ Kaptein, Judith van Paassen, MAM Stals, MV Huisman, et al. Incidence of thrombotic complications in critically ill icu patients with covid-19. *Thrombosis research*, 191:145–147, 2020. 2

[13] Marcel Levi, Jecko Thachil, Toshiaki Iba, and Jerrold H Levy. Coagulation abnormalities and thrombosis in patients with covid-19. *The Lancet. Haematology*, 7(6):e438, 2020. 2

[14] Lin Li, Lixin Qin, Zeguo Xu, Youbing Yin, and et al. Using artificial intelligence to detect covid-19 and community-acquired pneumonia based on pulmonary ct: Evaluation of the diagnostic accuracy. *Radiology*, 296:E65–E71, 2020. 2, 6

[15] M Ligero, G Torres, C Sanchez, and et al. Selection of radiomics features based on their reproducibility. In *Annu Int Conf IEEE Eng Med Biol Soc*, 2019. 4

[16] Yang Lu and Homer A Macapinlac. Perfusion spect/ct to diagnose pulmonary embolism during covid-19 pandemic, 2020. 2

[17] Wang M, Xia C, Huang L, and et al. Deep learning-based triage and analysis of lesion burden for covid-19: a retrospective study with external validation. *Lancet Digit Health*, 2(10):e506–e515, 2020. 2

[18] Dennis McGonagle, Kassem Sharif, Anthony O'Regan, and Charlie Bridgewood. The role of cytokines including interleukin-6 in covid-19 induced pneumonia and macrophage activation syndrome-like disease. *Autoimmunity reviews*, 19(6):102537, 2020. 2

[19] Ronald MS. Artificial intelligence of covid-19 imaging: A hammer in search of a nail. *Radiology*, 298:E169–E171, 2021. 2

[20] MWX Ooi, A Rajai, R Patel, N Gerova, V Godhamgaonkar, and SY Liong. Pulmonary thromboembolic disease in covid-19 patients on ct pulmonary angiography–prevalence, pattern of disease and relationship to d-dimer. *European Journal of Radiology*, 132:109336, 2020. 2

[21] Neo Poyiadji, Peter Cormier, Parth Y Patel, Mohamad O Hadied, Pallavi Bhargava, Kanika Khanna, Jeffrey Nadig, Thomas Keimig, David Spizarny, Nicholas Reeser, et al. Acute pulmonary embolism and covid-19. *Radiology*, 297(3):E335–E338, 2020. 2

[22] Zhang R, Qi Z Tie X, and et al. Diagnosis of covid-19 pneumonia using chest radiography: Value of artificial intelligence. *Radiology*, 2020. 6

[23] Das A et al. Selvaraju RR, Cogswell M. Grad-cam: Visual explanations from deep networks via gradient-based localization. In *ICCV*, 2017. 2

[24] Young Joo Suh, Hyunsook Hong, Mickaël Ohana, Florian Bompard, Marie-Pierre Revel, Clarissa Valle, Alban Gervaise, Julien Poissy, Sophie Susen, Guillaume Hékimian, et al. Pulmonary embolism and deep vein thrombosis in covid-19: A systematic review and meta-analysis. *Radiology*, page 203557, 2020. 2

[25] Joost JM van Griethuysen, Andriy Fedorov, Chintan Parmar, Ahmed Hosny, Nicole Aucoin, Vivek Narayan, Regina GH Beets-Tan, Jean-Christophe Fillion-Robin, Steve Pieper, and Hugo JWL Aerts. Computational radiomics system to decode the radiographic phenotype. *Cancer research*, 77(21):e104–e107, 2017. 4

[26] Naude W. Artificial intelligence vs covid-19: limitations, constraints and pitfalls. *Ai Soc*, page 1, 2020. 2

[27] Zhenguo Zhai, Chenghong Li, Yaolong Chen, Grigorios Gerotziafas, Zhenlu Zhang, Jun Wan, Peng Liu, Ismaïl Elalamy, Chen Wang, et al. Prevention and treatment of venous thromboembolism associated with coronavirus disease 2019 infection: a consensus statement before guidelines. *Thrombosis and haemostasis*, 120(6):937, 2020. 2

[28] Lionel S Zuckier, Renée M Moadel, Linda B Haramati, and Leonard M Freeman. Diagnostic evaluation of pulmonary embolism during the covid-19 pandemic. *Journal of Nuclear Medicine*, 61(5):630–631, 2020. 2